ISSN 0965-545X, Polymer Science, Series A, 2022, Vol. 64, No. 1, pp. 19–37. © Pleiades Publishing, Ltd., 2022.
ISSN 0965-545X, Polymer Science, Series A, 2022. © Pleiades Publishing, Ltd., 2022.
Russian Text © The Author(s), 2022, published in Vysokomolekulyarnye Soedineniya, Seriya A, 2022, Vol. 64, No. 1, pp. 24–44.

POLYMER GELS

Trends in Cryotropic Gelation of Semidilute Aqueous Solutions of Poly(vinyl alcohol) with Different Thermal History

E. A. Kurskaya[a,*], E. A. Podorozhko[a], E. S. Afanasyev[a], E. G. Kononova[a], and A. A. Askadskii[a,b]

[a] *Nesmeyanov Institute of Organoelement Compounds, Russian Academy of Sciences, Moscow, 119991 Russia*

[b] *Moscow State University of Civil Engineering, Moscow, 129337 Russia*

**e-mail: kurskaya_e@mail.ru*

Received July 6, 2021; revised September 8, 2021; accepted November 1, 2021

Abstract—Different trends observed during cryotropic gelation of 8% poly(vinyl alcohol) aqueous solutions (preheated to 25, 55, and 85°C) at rapid cooling and freezing of the system have been examined. The data of rheology, thermomechanical analysis, attenuated total reflection, and scanning electron microscopy have revealed that the macroporous poly(vinyl alcohol) cryogels formed under above conditions differ in elastoplastic properties, swelling ability in water, degree of microcrystallinity, and pores size. The obtained results have been confirmed by the study of diffusional release of stabilized silver nanoparticles from the cryogels. It has been shown that the macropores walls in the cryogel network consist of spherical formations, likely contacting microgel particles formed during the liquid-phase separation of the polymer solution prior to the cryotropic gelation stage.

DOI: 10.1134/S0965545X22010060

INTRODUCTION

Gelation of certain biocompatible, biodegradable, and nontoxic natural and synthetic water-soluble polymers is of interest for the study and diverse practical applications of gels. Poly(vinyl alcohol) (PVA) is among such polymers [1]. Physical hydrogels of PVA including macroporous cryogels [2] are thermoreversible amorphous-crystalline networks exhibiting upper critical solution temperature [3–6]. PVA gels have been widely used in food industry [7], in medicine as carriers for drug delivery [8] and wound dressings [9, 10], for the tendon injuries treatment [11, 12] and skin recovery [13] as well as in ophthalmology [14] and bioengineering [15, 16].

Successful application of PVA-based materials demands certain set of properties: stability under physiological conditions, tunable structural and mechanical parameters, hydration degree, and rate of drugs diffusion. These properties in many respects depend on molecular mass and degree of deacetylation of the macromolecules [17], their concentration in the solution, and temperature-kinetic conditions of the gels and cryogels formation [8, 18, 19].

Flexible PVA macromolecules bearing pendant hydroxyl functional groups are strongly hydrophilic and prone to the formation of intra- and intermolecular hydrogen bonds via donor as well as acceptor mechanisms [20]. Microcrystallinity typical of PVA does not prevent its swelling, yet restricts its dissolution in cold or warm water. PVA solubility is increased at temperature above 65°C—onset of the microcrystallites melting [21, 22]. To completely disrupt the PVA crystallites, it is dissolved at 120°C under autoclaving conditions [23]. The highest possible dissociation of supramolecular formation is thus realized along with sufficiently strong hydration of the macromolecules, decelerating the crystallization on cooling. The presence of the crystallization centers (nuclei) and the conditions favoring the ordering of macromolecular segments (parallel laying [24]) linked via intra- and intermolecular hydrogen bonds not involving water molecules [25, 26] are required to induce the crystallization.

Depending on concentration and temperature, semidilute aqueous solutions of PVA afford weak hydrogels via binodal macrophase separation of the polymer system or viscous opalescent sols via the spinodal microphase separation [27]. Strong thermally stable hydrogels can be prepared from concentrated polymer solution or via controlled dehydration of PVA macromolecules: water evaporation [9, 28], use of mixed aqueous-organic solvents [29], or introduction of salting-out low-molecular compounds into the aqueous medium [30].

Freezing out of the solvent is among the approaches to tune the dehydration of PVA macromolecules and obtain its thermally stable noncovalent gels. Cryotropic gelation includes several stages: freezing of an aqueous PVA solution to crystallize free and part of weakly bound water, keeping the system in the

frozen state, and thawing under the conditions favoring the formation of amorphous and crystalline nodes of the cryogel network. Morphology and physicochemical properties of the cryogels formed from aqueous solutions of the polymers (concentration $c \geq 5\%$) are affected by temperature and duration of each of the stages, rate of the temperature change, and the number of freezing-thawing cycles [31, 32]. The balance of amorphous and crystalline structure of PVA influences on their swelling ability, thermal stability, and structural-mechanical properties [33, 34].

It has been shown in [35] that heating of PVA solutions leads to the decrease in the thickness of the macromolecules hydrate shell. The number of hydrogen bonds between PVA macromolecules and water is reduced by about 1.2 times upon heating from 10 to 40°C [36]. Conformation state, intensity of the interaction between the hydrated macromolecules [37], and physical properties of free water (dynamic viscosity, self-diffusion, relaxation, and electrical conductivity) are temperature-dependent as well [38–41]. Rapid cooling of preheated aqueous PVA solutions below the glass transition temperature of the polymer and temperature of ice crystallization has allowed certain fixation of the system state formed during the preheating [42]. Further freezing of the polymer system leads to the formation of ice crystals [43] and concentrating of the macromolecules in the space between the crystals, and macroporous PVA cryogels are obtained upon thawing [44].

The influence of various temperature-duration parameters of cryostructuring of aqueous PVA solutions on the properties of the prepared cryogels have been comprehensively studied. However, insufficient attention has been given to the issue of thermal history of the starting solutions on the morphology and physico-chemical properties of the cryogels. That was the major aim of the study reported herein.

EXPERIMENTAL

Poly(vinyl alcohol) with $M = (11 \pm 1.5) \times 10^4$ and deacetylation degree about 100% (Aldrich) and silver nanoparticles (d = 50–60 nm) stabilized by amphiphilic macromolecules of ethylene–maleic acid copolymer (unit molecular mass 144) synthesized as described in [45] were used. The cryogels were prepared from the dry polymer and bidistilled water as follows. A 8% solution of PVA was prepared: polymer granules were swollen in water at room temperature during 18–20 h and heated at 90–95°C with stirring during 2 h until complete dissolution; upon the dissolution, the water volume was adjusted to compensate for evaporation. The solution and the formed hydrogel were kept at 8–10°C during no longer than two weeks to avoid the hydrogel macrosyneresis.

Temperature dependence of turbidity (light scattering at angle of 45° and wavelength 435 nm) of the starting 8% PVA sol was obtained using a Specol spectrophotometer (Germany) equipped with a PhoM3/19 photomultiplier and a TK constant-temperature cell. The measurements were performed over the 20–90°C temperature range with 5 degrees step. The PVA solution was equilibrated during 15 min at each temperature prior to the measurement.

To investigate the effect of preheating of the 8% PVA sols on the properties of the formed cryogels, 1.8 g of the starting sol was kept during 15 min at T = 25, 55, or 85°C in a 2-mL closed metal container and then immediately put to a freezer at $T = -13 \pm 2$°C. The rate of the loss of fluidity of the cooled specimens was of 4.8, 5.5, and 6.2 deg/min for the sols with the starting temperature 25°C and the solutions preheated at 55 and 85°C, respectively.

The solutions were kept in the freezer during 18 h. Thawing of the frozen system was performed either with short keeping at the temperature of the system devitrification (determined from the TMA curves): 1 h at T = 10°C and 1 h at $T \approx 23$°C or with longer keeping: 24 h at T = 10°C and 1 h at $T \approx 23$°C. The number of the freezing–thawing cycles n was varied between 1 and 3. Thawing between the cycles was performed in the fast mode.

Structural-mechanical properties of the PVA cryogels upon thawing and keeping during several days in a humid atmosphere (dessicator, $T \approx 23$°C) were investigated using a Kargin–Sogolova dynamometric balance [46] equipped with a spherical punch (ball diameter 4 mm). The conditional-instantaneous shear modulus G_0 and shear compliance at 15 min upon the system unloading J_{15} was calculated using the equation from [47]:

$$G_0 = (3/16)\,P/(R^{0.5}h^{1.5}), \quad J_{15} = 1/G_{15},$$

with P being the load (N), R being the indenter radius (m), and h being the depth of the indenter immersion in the gel (m). The $J_{15} = 1/G_{15}$ parameter was obtained from the creep curves (the time dependence of the deformation under constant load and upon unloading of the cryogel specimens).

To assess kinetics of the cryogels mass m_t change with respect to the initial mass m_0 during swelling at room temperature, the specimen mass was monitored during keeping in 3.5 mL of bidistilled water. The specimens solubility was determined by refractometry, measuring the concentration and mass of the cryogel portion dissolved in 3.5 mL of water p_t with respect to the initial specimen mass p_0. The calibrating curve relating the PVA concentration in an aqueous solution and its refractive index was obtained at T = 25°C.

Concentration of silver nanoparticles stabilized with the ethylene–maleic acid copolymer diffused from the filled macroporous PVA cryogels into water was determined by means of visible-range spectrophotometry [48]. The nanocomposite PVA cryogels were

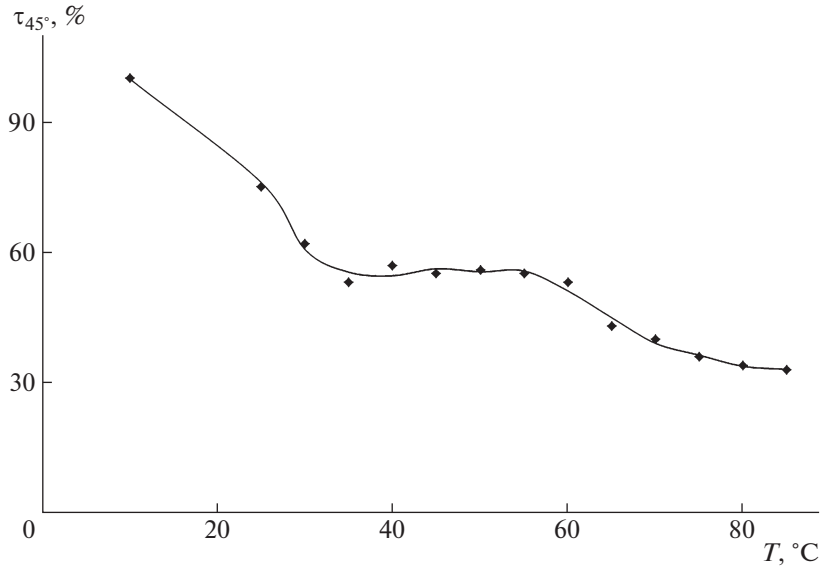

Fig. 1. Turbidity of 8% PVA sol measured at angle of 45° as a function of temperature.

prepared as follows. 1.5 μmol of the nanoparticles as aqueous sol was added to the 8% solution of PVA preheated during 15 min at the desired temperature. The mixture was stirred, immediately frozen at −13°C during 18 h, and thawed at 10°C during 24 h. The cryogel specimen was then put in 3.5 mL of bidistilled water, and the silver nanoparticles concentration was determined in the solution daily by measuring the absorbance D at wavelength 410 ± 5 nm. The concentration was determined using the $C(\mu mol/mL) = kD_{410}$ nm calibration with $k = 0.154$ [45]. The stabilized silver nanoparticles were not noticeably aggregated during the preparation of the nanocomposite PVA cryogels under the chosen conditions, as evidenced no significant variation of the position of the absorption maximum in the silver sol spectrum (410 ± 5 nm) before and after freezing–thawing of the system (during diffusion of the nanoparticles from the PVA cryogels to the aqueous medium) [48].

Thermomechanical analysis of the cryogels was performed using a Q400EM instrument (TAInstruments, USA); the specimens were heated from −40°C to 90°C at 5 deg/min rate, the compression force was 0.6 N and the indented diameter was 6 mm.

ATR IR spectra of the PVA cryofilms with different thermal history of the starting solution were recorded using a dried one at Bruker Vertex 70v IR spectrometer (Bruker, Germany) equipped with a diamond prism, upon the specimens drying at room temperature.

The cryogels specimens for the investigation by means of electron microscopy were prepared as described elsewhere [43]. The samples were treated with a 2.5% solution of glutaric aldehyde in 0.1 M HCl and washed with water. Water in the specimens was exchanged with ethanol via successive treatment with the solutions with increasing fraction of the alcohol, then the samples were washed three times with acetone and dried under the critical point conditions. Each specimen was then immersed into liquid nitrogen and fractured in the direction perpendicular to the ice crystals growth. The cleavage surface was layered with aluminum (thickness 250 Å) in an argon medium using an IB-3 ionic sprayer (Eiko Engineering, Japan). The specimens structure was observed with 3500× and 10000× magnification using a Camscan S-2 electron microscope (Cambridge Instruments, Great Britain) operating at accelerating voltage of 20 kV.

RESULTS AND DISCUSSION

Keeping of the 8% solution of PVA at low positive temperature resulted in the formation of opalescent hydrogel with melting point of 18°C [49]. Such gel was slowly converted into viscous opalescent sol when kept at room temperature. The remaining associates of macromolecules stabilized mainly by the hydrogen bonds between the polymer hydroxyl groups were the light scattering sites in that sol. The decrease in turbidity of the system with the increase in temperature qualitatively reflected the decreasing size of the associates (Fig. 1). The decrease in the opalescence intensity at 35–60°C corresponded to the rupture of weak intermolecular hydrogen bonds, whereas the hydrophobic interactions between the nonpolar fragments of the amphiphilic PVA chains as well as the nuclei of microcrystallites (formed during keeping of the starting 8% hydrogel at low positive temperature) were likely disrupted at temperature above 60°C (Fig. 2).

Analysis of the PVA–water phase diagram [49] revealed that 8% solution of PVA ($M \sim 10^5$) was a liquid two-phase microgel system (i.e. corresponded to

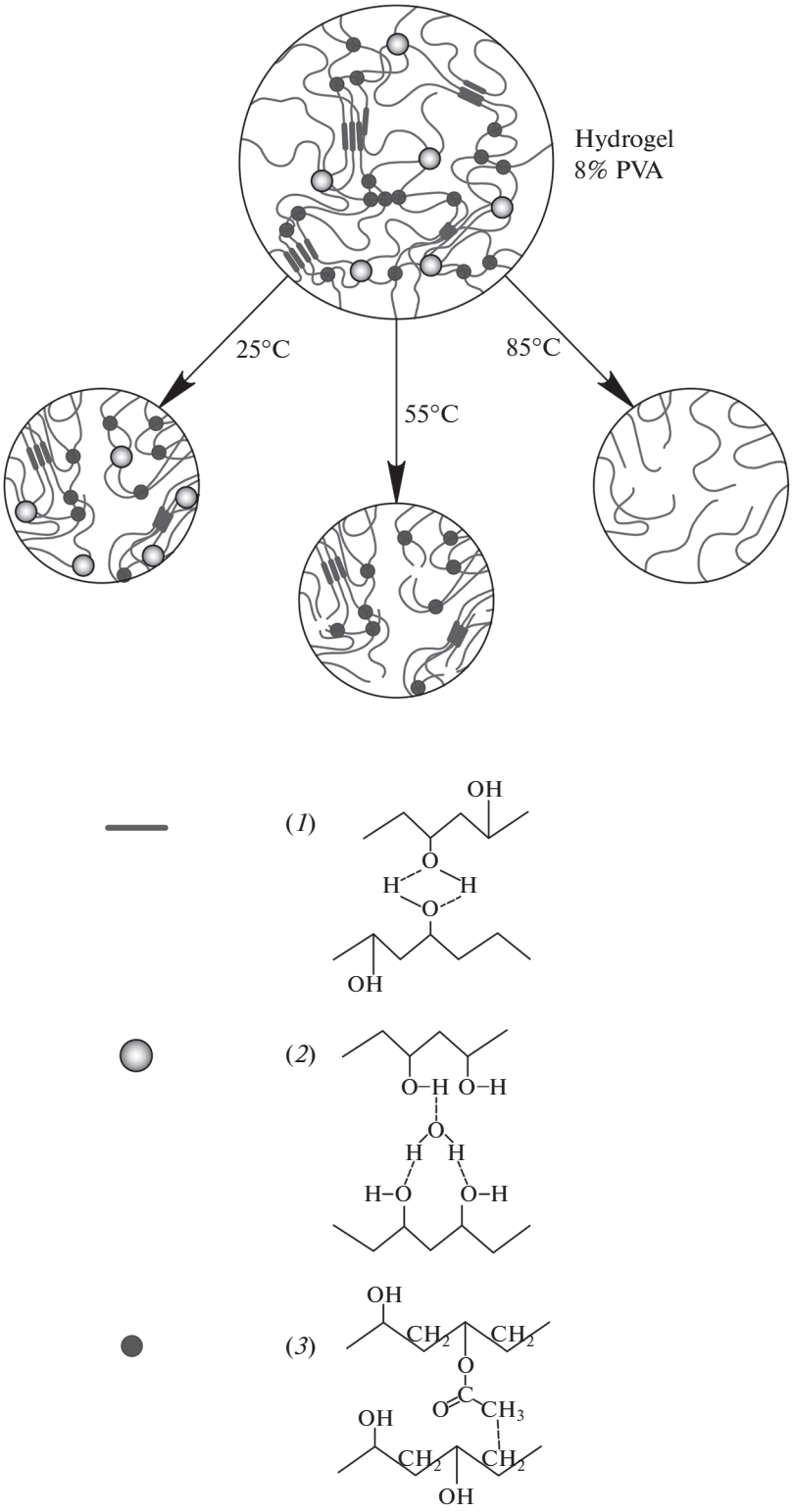

Fig. 2. The effect of heating on dissociation of the intermolecular bonds in 8% PVA hydrogel. *1*—hydrogen bonds between hydroxyl groups of the macromolecules in the microcrystallite regions, not involving water molecules, *2*—hydrogen bonds in the amorphous regions, through water layer, *3*—hydrophobic interactions between nonpolar groups of the macromolecules.

the diagram region between the binodal and spinodal lines) at 25°C; the PVA solution contained the macromolecules associates (corresponding to the region above the binodal line) at 55°C, whereas the PVA solution at 85°C contained mainly individual macromolecules. It was suggested that rapid cooling and

Table 1. The influence of ageing at ~23°C on the conditional-instantaneous shear modulus G_0 and residual deformation J_{15} of the cryogels prepared with a single ($n = 1$) freezing and thawing the system at 10°C during 1 h

Temperature of preheating of starting solution, °C	Ageing duration, days	G_0, kPa	ΔG_0, kPa	J_{15}, kPa^{-1}
25	0	2.5/2.0	0.5	0.10/0.15
	1	2.4/1.8	0.6	0.22/0.28
	5	1.6/1.3	0.4	0.79/0.84
55	0	2.7/1.9	0.8	0.23/0.26
	1	2.4/2.1	0.3	0.26/0.33
	5	1.6/1.3	0.3	0.44/0.60
85	0	2.4/1.8	0.6	0.41/0.53
	1	2.1/2.0	0.1	0.35/0.40
	5	1.9/1.9	0	0.48/0.50

Here and in Tables 2, 3 G_0 and J_{15} are given as follows: the numerator is the value for the bottom side of the specimen, the denominator is the value for the upper side of the specimen; ΔG_0 is the difference between the G_0 values for the bottom and the upper sides of the specimen. Accuracy of G_0 and J_{15} determination was ± 0.2 kPa and ± 0.05 kPa^{-1}, respectively.

Table 2. The influence of ageing at ~23°C on the conditional-instantaneous shear modulus G_0 and residual deformation J_{15} of the cryogels prepared with a single ($n = 1$) freezing and thawing the system at 10°C during 24 h

Temperature of preheating of starting solution, °C	Ageing duration, days	G_0, kPa	ΔG_0, kPa	J_{15}, kPa^{-1}
25	0	1.4/1.2	0.2	0.50/0.56
	1	1.6/1.5	0.1	0.33/0.36
	5	2.1/1.9	0.2	0.14/0.19
55	0	1.8/1.6	0.2	0.52/0.58
	1	1.9/1.7	0.2	0.31/0.36
	5	2.1/2.0	0.1	0.13/0.18
85	0	1.4/1.3	0.1	0.43/0.46
	1	1.6/1.5	0.1	0.23/0.26
	5	2.2/2.2	0	0.15/0.18

freezing of the PVA aqueous solutions with different thermal history and, hence, differing in the degree of assembly of the macromolecular structures, could afford the cryogels with different morphology and physico-chemical properties. The cryogels formed from the PVA solution upon preheating at 25, 55, and 85°C are denoted as CG-25, CG-55, and CG-85, respectively.

Elastoplastic Properties of the Cryogels Formed from PVA Solutions with Different Thermal History

The CG-25, CG-55, and CG-85 cryogels formed via single ($n = 1$) freezing–thawing followed by the system keeping at 10°C during 1 (Table 1) and 24 h (Table 2) were similar in opacity and exhibited pronounced elastic properties as well as strong adhesion to hydrophilic surfaces. Since the freezing process was predominantly unidimensional (the temperature gradient was directed from the cooling surface below to the upper part of the specimens), certain nonuniformity of the structural-mechanical properties over the freshly prepared cryogels volume could be expected.

Tables 1 and 2 list the values of the conditional-instantaneous shear modulus G_0 and residual shear deformation 15 min after the unloading J_{15} measured at both bases of the cylindrical specimens. Analysis of the obtained data led to the conclusion that the elastoplastic properties of the cryogels were mainly affected by the duration of their thawing at low positive temperature rather than by the thermal history of the starting PVA solutions. For example, the G_0 values for the CG-25, KG-55, and KG-85 samples upon thawing were insignificantly different. However, room-temperature ageing of the cryogels kept at 10°C during 1 h

Table 3. Conditional-instantaneous shear modulus G_0 and residual deformation J_{15} of the PVA cryogels prepared with thrice-repeated ($n = 3$) freezing and thawing the system at 10°C with short (1 h) keeping between the cycles

Temperature of preheating of starting solution, °C	Ageing duration at ~23°C, days	G_0, kPa	ΔG_0, kPa	J_{15}, kPa^{-1}
25	1	6.8/5.2	1.6	0.28/0.43
	5	6.8/5.7	1.1	0.21/0.28
55	1	7.0/5.8	1.2	0.25/0.35
	5	7.9/6.9	1.0	0.10/0.17
85	1	7.0/6.8	0.2	0.13/0.18
	5	8.2/7.8	0.4	0.13/0.23

led to decrease in G_0 (Table 1), in contrast to the samples kept at 10°C during 24 h (Table 2). On the contrary, the residual deformation J_{15} values were increased during ageing of the cryogels obtained with short keeping (Table 1) and decreased for the samples prepared with longer keeping (Table 2). In the latter case, the G_0 values became even over the specimen volume faster (Table 2).

The nucleation and growth of microcrystallites with the formation of relatively thermally stable crosslinks of the gel network appearing via the interaction of segments of different macromolecules were possible at low positive temperature corresponding to devitrification of the polymer system. This process was slow [75] and required longer duration in comparison with the formation of less thermally stable amorphous contacts between the hydrated functional groups of the macromolecules. That fact was evidently the reason why longer keeping of the samples at 10°C favored the formation of more elastic and less plastic cryogels.

When two or three freezing–thawing cycles ($n = 2$ or 3) were performed, the CG-25, CG-55, and CG-85 samples revealed more dense white coloration and no adhesion to hydrophilic surfaces in comparison to the systems subject to single freezing–thawing. Comparison of the corresponding G_0 and J_{15} values (Tables 1 and 3) revealed significant increase in the value of the conditional-instantaneous elasticity modulus and the decrease in the residual deformation J_{15} of the CG-25, CG-55, and (especially) CG-85 samples with the increase of the cycles number n to 3. The obtained data did not contradict the results of other studies of PVA cryogels [50]. The observed changes were due to compacting and strengthening of the walls of the cryogel network under conditions of the macromolecules concentrating in the space between the ice crystals during the cryogenic impact.

Investigation of the Cryogels Swelling Ability in Water

Analysis of the swelling of PVA cryogel allowed comparison of their hydration depending on the conditions of the samples formation. We determined the change in the mass of the PVA cryogels ($n = 1$) during keeping in water during 7 days at room temperature, with reference to the initial mass (accounting for the possibility of the soluble polymer fraction transfer into the aqueous phase. In the case of the CG-85, CG-55, and CG-25 samples formed with short (1 h) keeping at 10°C, the ratio of the swollen cryogel mass and the initial one m_t/m_0 was increased, i.e. the swelling prevailed over partial dissolution (Fig. 3a). High m_t/m_0 values were observed for the hydrogels formed with long (24 h) keeping at 10°C (Fig. 3b). The highest relative increase in the mass during swelling (of 140–150%) was marked for the CG-85 samples. High temperature of the starting solution preheating before the freezing led to partial dehydration of the PVA macromolecules, which, in combination with prolonged keeping of the thawed samples at low positive temperature with a single freezing–thawing cycle ($n = 1$), favored the formation of cryogels with high swellability.

At $n = 1$, solubility in water of the PVA cryogels with different thermal history of the starting solution did not exceed 2.3–3.0% of the starting mass (Fig. 4a).

The increase in the number of the freezing–thawing cycles to three ($n = 3$) led to the decrease in the swelling degree (Fig. 3c) and solubility in water (Fig. 4b) for the studied cryogel types. Those data evidenced the formation of additional crosslinks in the cryogel network, which restricted the swelling and dissolution.

Thermomechanical Analysis of the Cryogels with Different Thermal History of the Starting Solution

The TMA method was used for the investigation of thermomechanical behavior of the CG-25, CG-55, and CG-85 samples at constant compressive loading. Fig. 5 displays integral and differential TMA curves (deformation as a function of temperature) for the CG-25, CG-55, and CG-85 samples formed with a single freezing–thawing cycle ($n = 1$) and short (1 h) duration of the thawed system at 10°C. The TMA curves of the marked samples showed a transition from the glassy state into the viscoelastic one at about 10°C (Fig. 5a) with the extremum in the differential curve at about 16–17°C (Fig. 5b). The second extremum at about 36°C revealed the transition of the viscoelastic sample into the viscous-flow state due to the rupture of the hydrogen bonds in the crosslinks of the cryogels network. It should be noticed that the transitions at higher temperature (above 60°C) characterizing the onset of disruption of the microcrystallites in the cryogels network were not observed in the TMA curves of the CG-25, CG-55, and CG-85 ($n = 1$) samples.

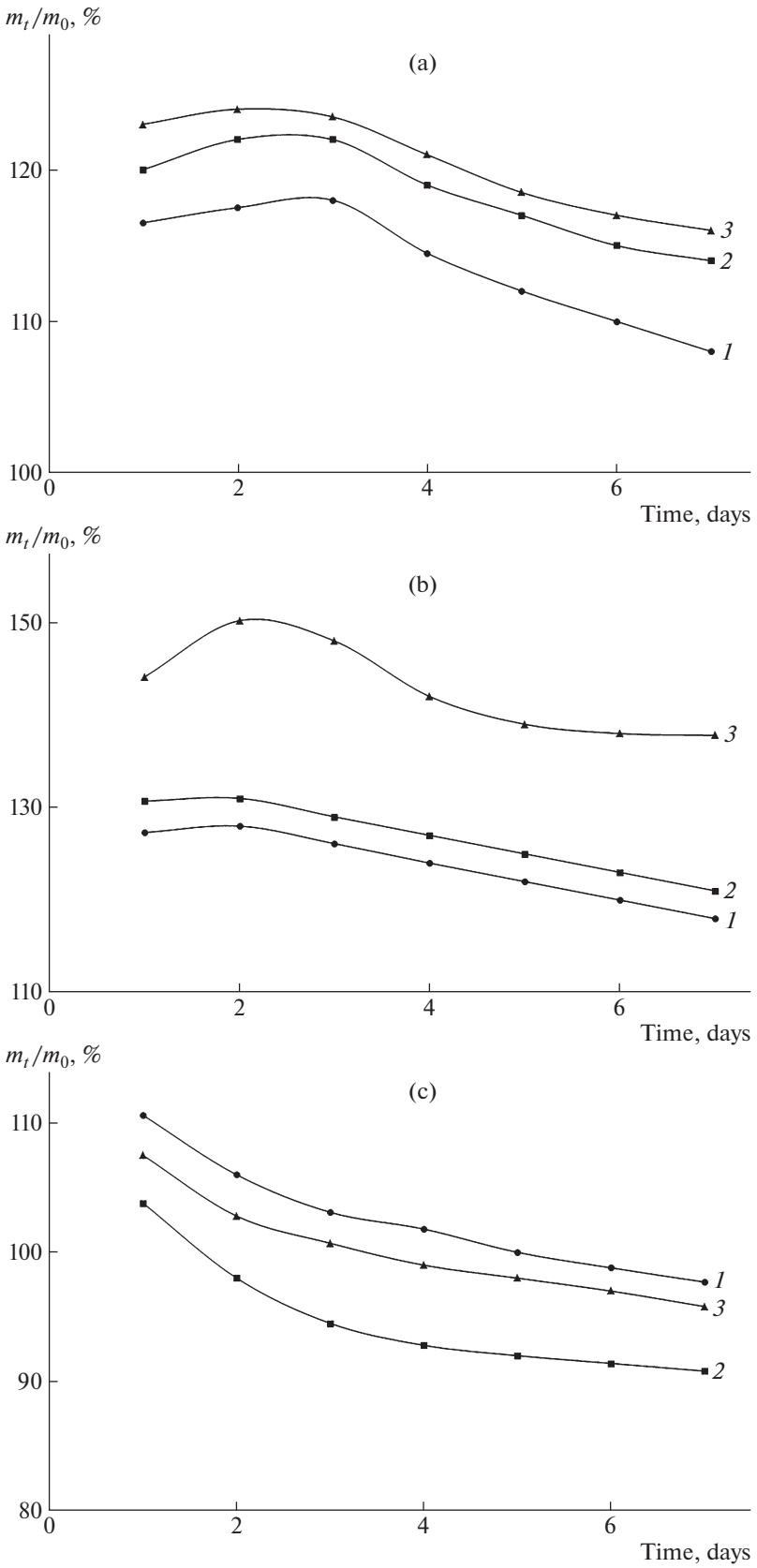

Fig. 3. Evolution of the ratio between the mass of cryogel swelling in water at (≈ 23°C) m_t to its initial mass m_0 for the CG-25 (*1*), CG-55 (*2*), and CG-85 (*3*) samples prepared with thawing at 10°C during 1 h and $n = 1$ (a), thawing at 10°C during 24 h and $n = 1$ (b), and thawing at 10°C during 1 h and $n = 3$ (c).

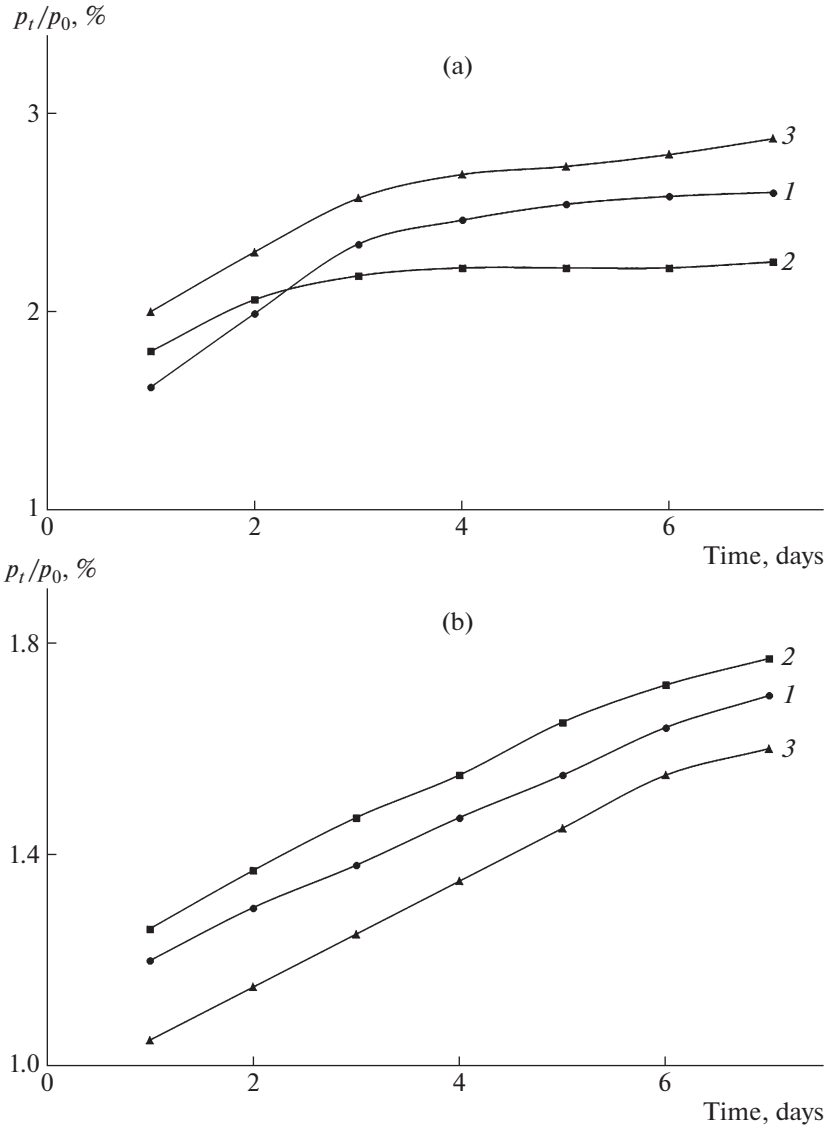

Fig. 4. Evolution of the ratio between the mass of cryogel dissolved in water p_t to its initial mass p_0 for the CG-25 (*1*), CG-55 (*2*), and CG-85 (*3*) cryogels prepared with thawing at 10°C during 1 h and n = (a) 1 and (b) 3 freezing–thawing cycles.

Similar TMA experiments were performed for the CG-25, CG-55, and CG-85 samples formed with two freezing–thawing cycles ($n = 2$) and short keeping at 10°C between the cycles (Fig. 6). In comparison with the results presented in Fig. 5, the integral TMA curves were changed for the CG-25 and CG-55 samples (Fig. 6a): the region of weak dependence of deformation on temperature marking the high-elasticity specimen state appeared at 40–60°C, and high-temperature transition into the viscous-flow state reflecting the melting of the microcrystallites in the network crosslinks was observed at about 70°C. Those features were not observed in the TMA curves for the CG-85 sample.

It should be noticed that at $n = 2$ even the decrease in the freezing temperature from −13 to −30°C (Fig. 7) did not induce the appearance of the microcrystallites in the crosslinks of the CG-85 network at short (curve *1*) and long (curve *2*) keeping of the thawed system at the devitrification temperature, 10°C. Those data could indirectly evidence the importance of the enhanced pressure during the formation of ice crystals for the elimination of weakly bound water molecules, the process favoring the formation of microcrystallites nuclei during the cryogenic impact on the polymer system.

The marked feature of the TMA curve for the CG-85 sample could be explained by the fact that the preheating of the starting PVA solution at 85°C led to disruption of most of the intra- and intermolecular hydrogen bonds as well as hydrophobic interactions and the microcrystallites nuclei which could have

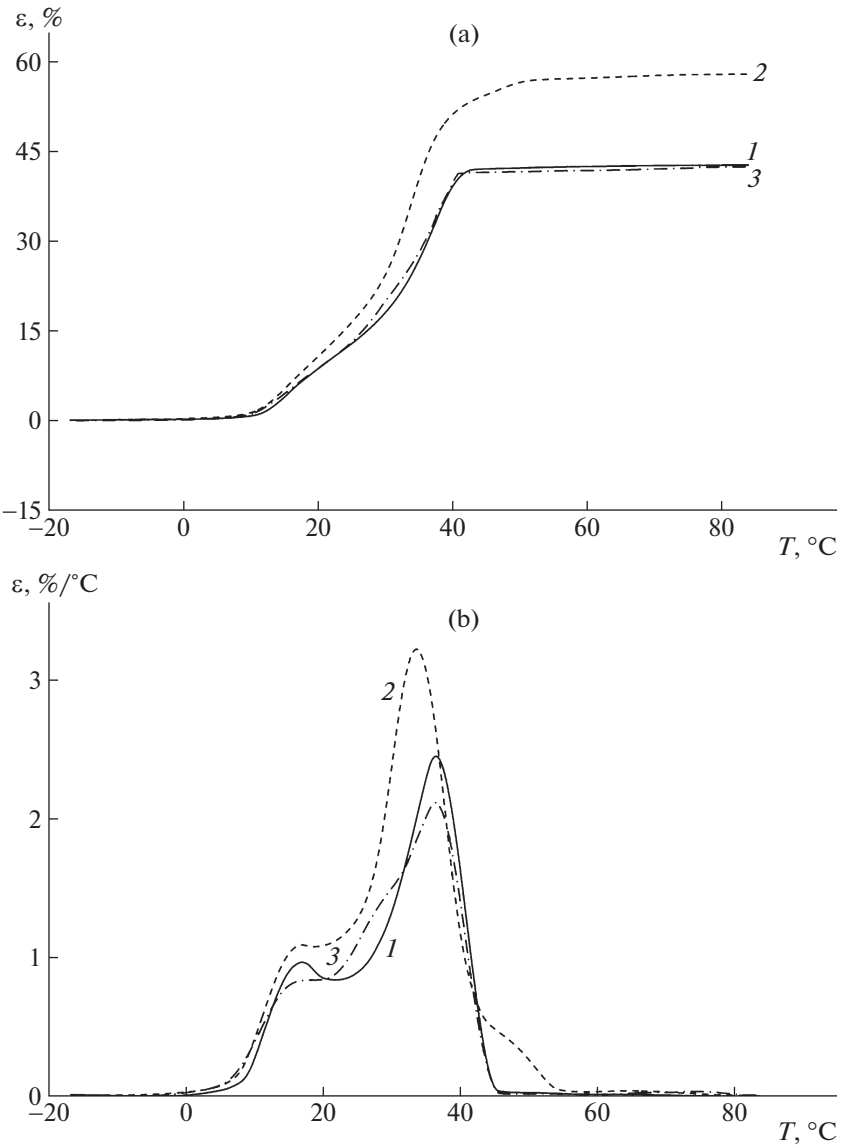

Fig. 5. Integral (a) and differential (b) TMA curves for the CG-25 (*1*), CG-55 (*2*), and CG-85 (*3*) cryogels prepared via single freezing at −13°C and thawing at 10°C during 1 h.

appeared in the initial 8% PVA hydrogel at low positive temperature. Fast cooling of the hot solution evidently was not accompanied by the formation of many new nuclei—centers of the microcrystallites growth.

Similar observations have been reported in the DSC study of 5% PVA cryogels subject to several freezing–thawing cycles [51]. The fraction of microcrystallites has not been manifested in the curve upon the first freezing-thawing cycle. The starting PVA solution has not contained the microcrystallites nuclei, since it has been prepared at 120°C under autoclaving conditions. At the same time, the NMR data have revealed that the 10% PVA solutions prepared under milder conditions (at 80°C) and cooled to room temperature contain about 5% of the primary microcrystallites which have favored further crystals formation in the samples under the cryogenic impact. Therefore, the obtained cryogels have exhibited high melting point (about 80°C) already upon the first freezing–thawing cycle [21].

Upon the third freezing–thawing cycle, the integral TMA curves (Fig. 8a) for all of the PVA samples considered in our study, CG-25, CG-55, and CG-85, revealed the high-temperature transition of the viscoelastic state into the viscous-flow one and the corresponding extremum in the differential curves at about 70°C reflecting the melting of the microcrystallites in the crosslinks of the cryogels network (Fig. 8b). It has been earlier found [54] that the increase in the number of the freezing–thawing cycles of the polymer solu-

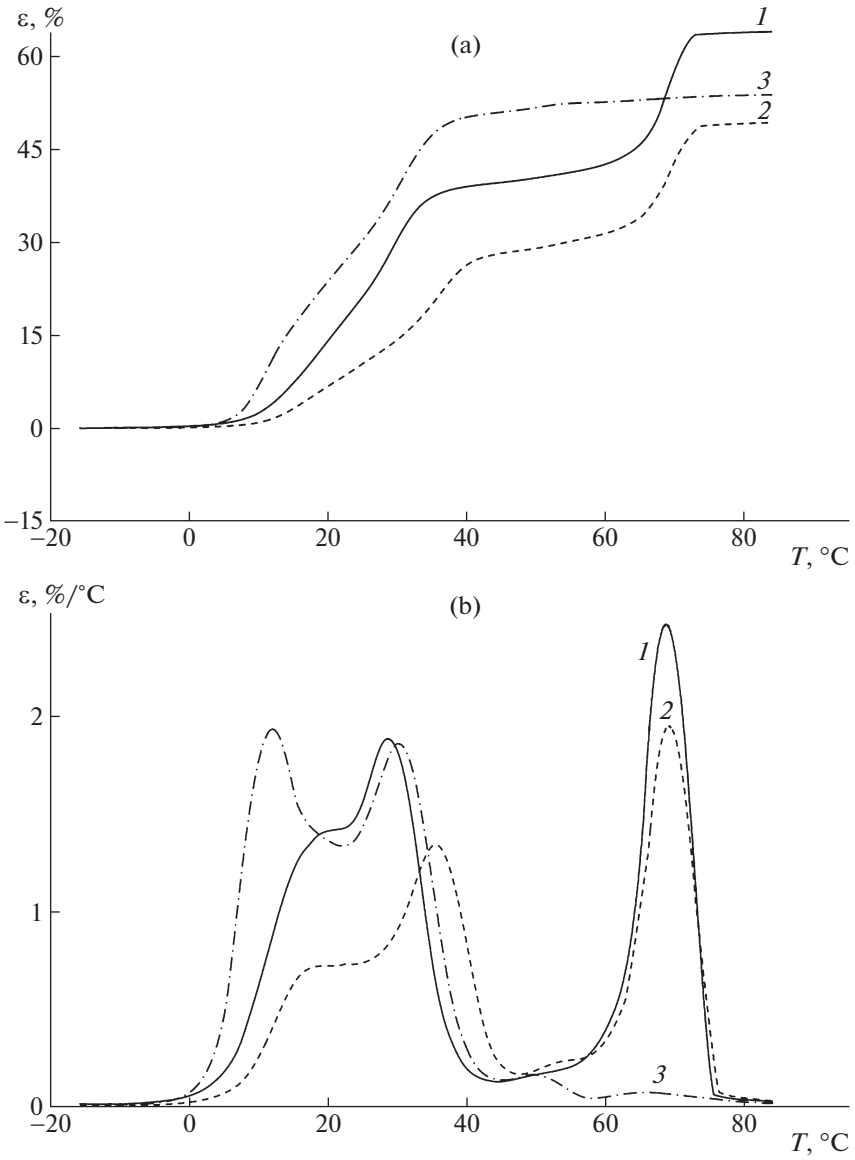

Fig. 6. Integral (a) and differential (b) TMA curves for the CG-25 (*1*), CG-55 (*2*), and CG-85 (*3*) cryogels prepared via twice freezing at −13°C and thawing at 10°C during 1 h.

tions led to the increase in the fraction of free (freezable) water, due to the partial transformation of the weakly bound water into the free one [52]. That phenomenon could result in the enlargement of the ice crystals and the increase in pressure in the space between them, promoting further concentrating of the polymer phase, strengthening of the cryogel walls, and the appearance of the microcrystallite nuclei under the favorable conditions [54].

Analysis of the ATR IR Spectra of the PVA Cryofilms Formed from the Solutions Differing in Thermal History

The content of free water and degree of crystallinity of PVA cryogels and the dried gels (cryofilms) are strongly different [55]. The IR spectroscopy data allows fairly accurate determination of a system crystallinity [56]. However, the presence of large amount of water (more than 80%) in the hydrated samples complicates the estimation. Therefore, only comparative analysis of the amount of the bound water and the characteristics of the hydrogen bonds was possible using the dried cryofilms prepared from the PVA solutions differing in thermal history.

The OH stretching bands at 3700–3000 cm^{-1}, their deformation band (1670–1600 cm^{-1}), and the C–H stretching band (3000–2900 cm^{-1}) in the ATR IR spectra were analyzed.

Let us first consider the case of single freezing–thawing cycle. Analysis of intensity of the bands in the

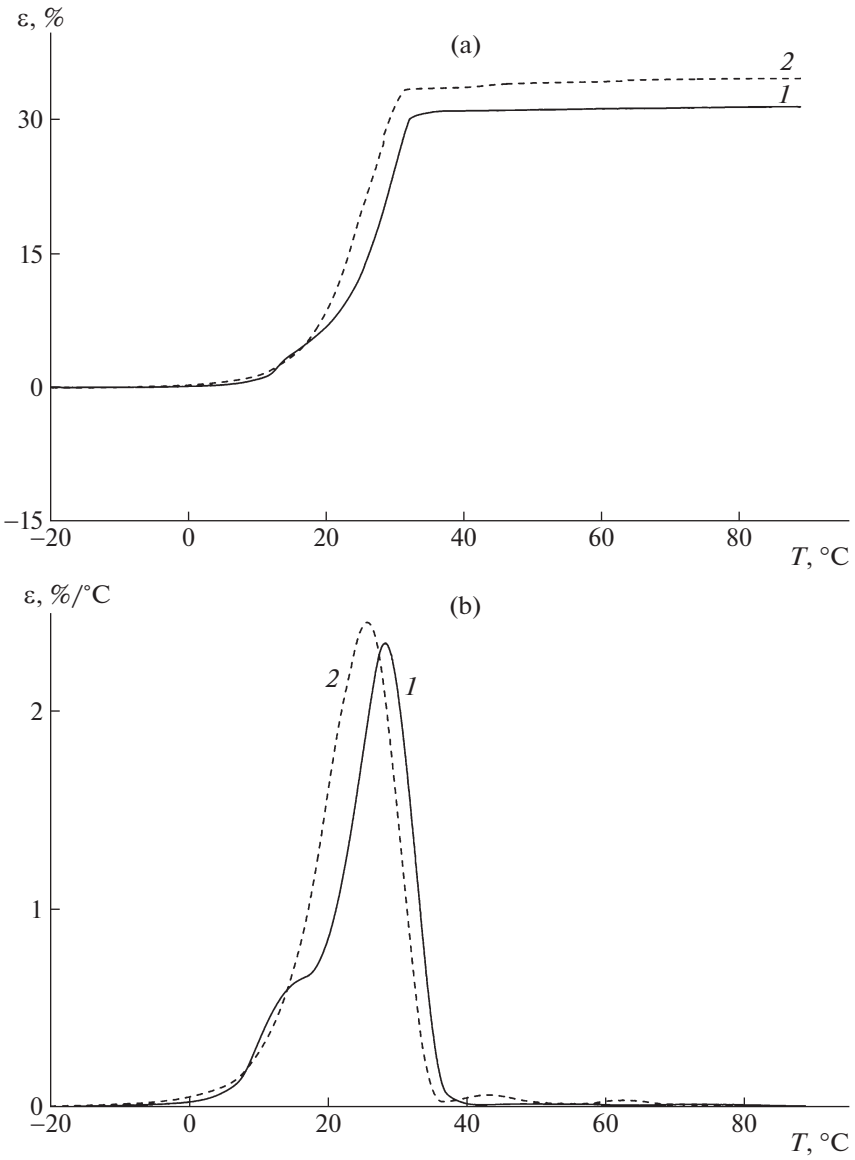

Fig. 7. Integral (a) and differential (b) TMA curves for the CG-85 cryogels prepared via twice freezing at −30°C and thawing at 10°C during 1 h (*1*) and 24 h (*2*).

regions of stretching 3700–3000 cm^{-1} and deformation 1670–1600 cm^{-1} vibrations of the OH groups (Fig. 9a) revealed that the content of the bound water in the CG-55 and CG-85 films was about twice lower than in the CG-25 one. It is known that the maximum of the OH deformation band for free water is found at 1637 cm^{-1}. In the case of the cryofilms, the water band was observed at higher frequency (1655 cm^{-1} for CG-25, 1670 cm^{-1} for CG-55 and CG-85). That fact pointed out that water in the considered samples constituted the hydrate shell of the PVA macromolecules (Fig. 9c).

Analysis of the half-width of the OH stretching band (3700–3000 cm^{-1}) showed that the macromolecules packing in the CG-25 sample (the OH band half-width 225 cm^{-1}) was the densest (that with the least differentiation of the hydrogen bonds). Half-width of than band in the spectra of the CG-55 and CG-85 samples was 275 and 350 cm^{-1}, respectively, evidencing less ordering of the system (Fig. 9b). The increase in the half-width of the OH stretching band in the spectra of the CG-85 and CG-55 samples in comparison with the CG-25 one was due to the formation of stronger intermolecular hydrogen bonds.

According to the ratio of the intensity of the C–H stretching bands (2939 and 2909 cm^{-1}), the content of different conformers of the macromolecules in the films was also dependent on the temperature of preheating of the starting PVA solution. Whereas the conformer characterized by the CH band at 2939 cm^{-1}

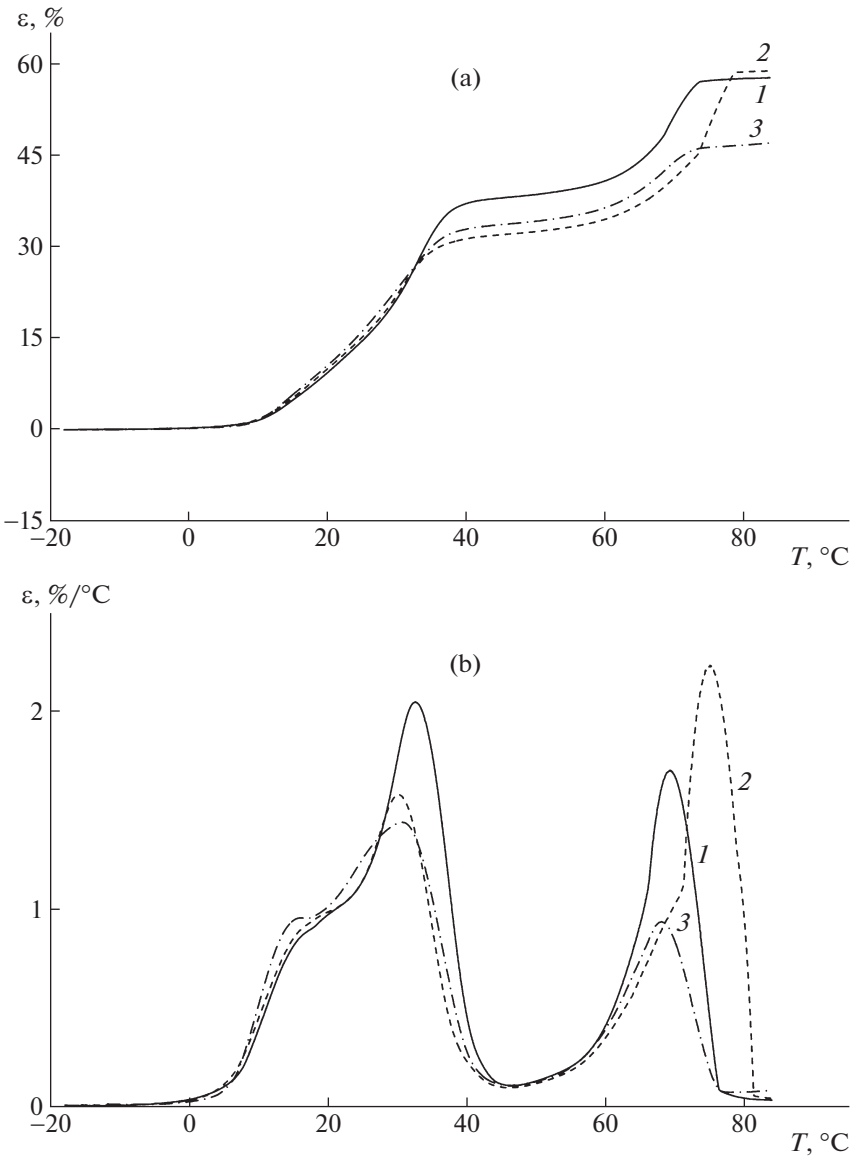

Fig. 8. Integral (a) and differential (b) TMA curves for the CG-25 (*1*), CG-55 (*2*), and CG-85 (*3*) cryogels prepared via thrice freezing at −13°C and thawing at 10°C during 1 h.

prevailed in the CG-25 sample, practically equal content of two conformers was found in the CG-55 and CG-85 samples, as evidenced by the presence of two CH bands of equal intensity in the spectra, at 2939 and 2909 cm^{-1}.

As revealed by the ATR IR spectroscopy data (Fig. 10), repeated freezing of the PVA cryogels enhanced the dehydration of the cryofilms in comparison with the samples upon single cryogenic impact. Analysis of the half-width of the OH groups stretching band (3700–3000 cm^{-1}) showed that at $n = 2$ the ordering of the structure of the CG-25 (290 cm^{-1}) and CG-55 (325 cm^{-1}**)** was improved, whereas the band half-width in the spectrum of the CG-85 sample (350 cm^{-1}) was not changed. That observation was in line with the behavior of the CG-25 and CG-55 samples ($n = 2$) in the TMA experiment. Moreover, the maximum of the OH stretching band was shifted to lower frequency (CG-25—3300 cm^{-1}, CG-55—3320 cm^{-1}, CG-85—3270 cm^{-1}) in comparison of the samples upon the first freezing–thawing cycle. That change could reflect the strengthening of the bonds in the polymer networks. Since the content of the bound water in the CG-85 sample was minimal, many of the hydrogel bonds were formed via the intermolecular interactions.

The conformer corresponding to the CH band at 2939 cm^{-1} prevailed in the densest structure (the CG-25 sample). The increase in temperature of the starting solution preheating (the CG-55 sample) led to

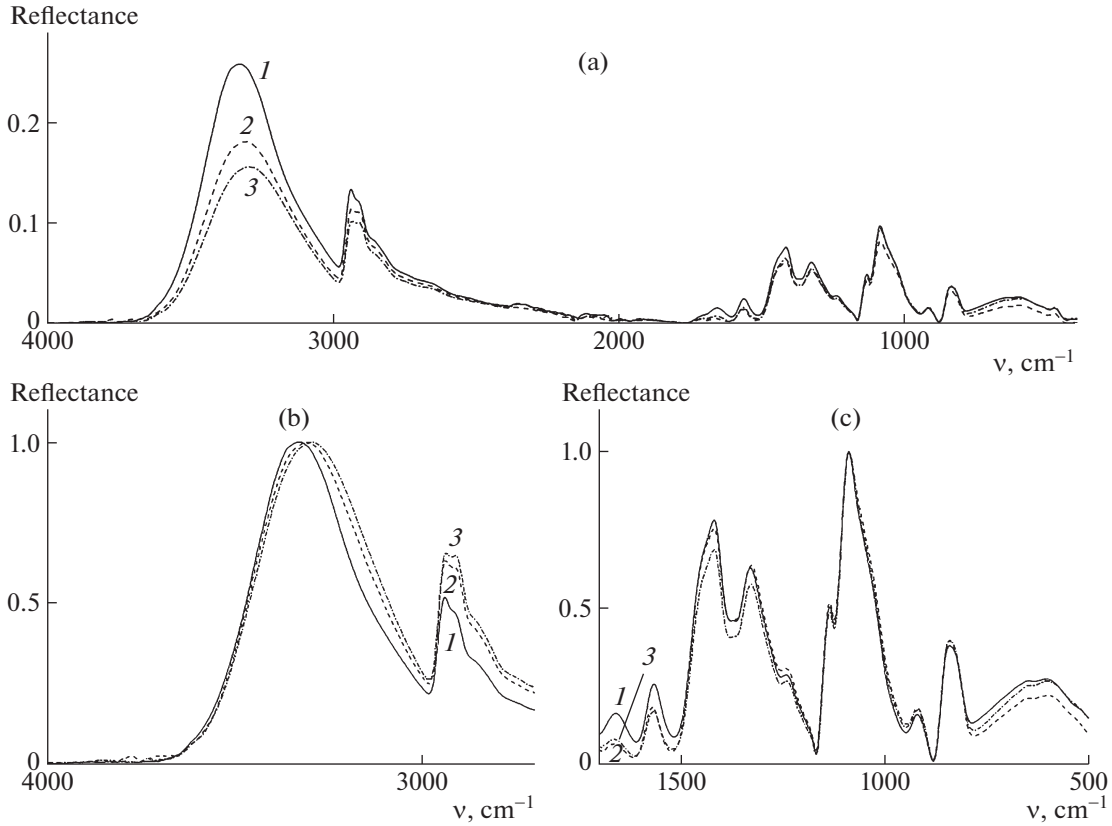

Fig. 9. (a) ATR spectra of the CG-25 (*1*), CG-55 (*2*), and CG-85 (*3*) samples prepared with a single freezing–thawing cycle ($n = 1$); (b) region of the OH (3700–3000 cm^{-1}) and C–H (3000–2900 cm^{-1}) groups stretching; c: region of the OH groups deformational vibrations, 1670–1600 cm^{-1}.

the strengthening of the second CH band at 2909 cm^{-1}, which became stronger than that at 2939 cm^{-1} in the spectrum of the CG-85 sample.

The increase in the number of the freezing–thawing cycles enhanced the observed effects related to the polymer network formation. Differentiation of the hydrogen bonds was reflected in the half-width of the OH groups band at 3700–3000 cm^{-1}, which was changed from 350 to 375 cm^{-1} for the CG-85 sample. That fact evidenced the strengthening of the hydrogen bonds and, hence, the formation of stronger polymer structure in comparison with the samples obtained with lower temperature of the starting solution preheating or with less of freezing–thawing cycles.

In summary, analysis of the ATR IR spectroscopy data concluded that the temperature of the PVA solution preheating affected the conformational state of the macromolecules in the cryogenic structures as well as regularity and strength of the forming hydrogen bonds. More disordered (due to preheating at 85°C) macromolecules afforded more regular network of the intermolecular hydrogen bonds, which was more prominently strengthened upon cyclic cryogenic impact.

Morphology of the PVA Cryogels Formed from the Solutions Differing in Thermal History

Since macroporous networks were formed via the cryotropic gelation of the 8% PVA solution, the cryogels morphology was mainly determined by the temperature-duration conditions of water crystallization and the frozen system thawing. Starting temperature of the polymer solution subject to fast cooling affected the freezing kinetics and morphology of the porous PVA cryogels as well.

Figure 11 displays the electron microscopy images of the PVA cryogels obtained from the solutions preheated at 25, 55, and 85°C ($n = 1$) as well as the solution preheated at 85°C ($n = 3$) via freezing at −13°C and keeping at 10°C during 24 h. The PVA cryogels were fractured in the direction perpendicular to the main direction of the ice crystals growth. Morphology of the CG-25 (Fig. 11a) and CG-55 (Fig. 11c) samples was typical of the macroporous cryogel matrix [44]. Apparently, hydrogen bonds of the macromolecules disrupted via preheating of the PVA starting solution at 55°C [27] could be partially restored during further cooling. That suggestion could explain similar morphology of the CG-25 and CG-55 samples. The size of

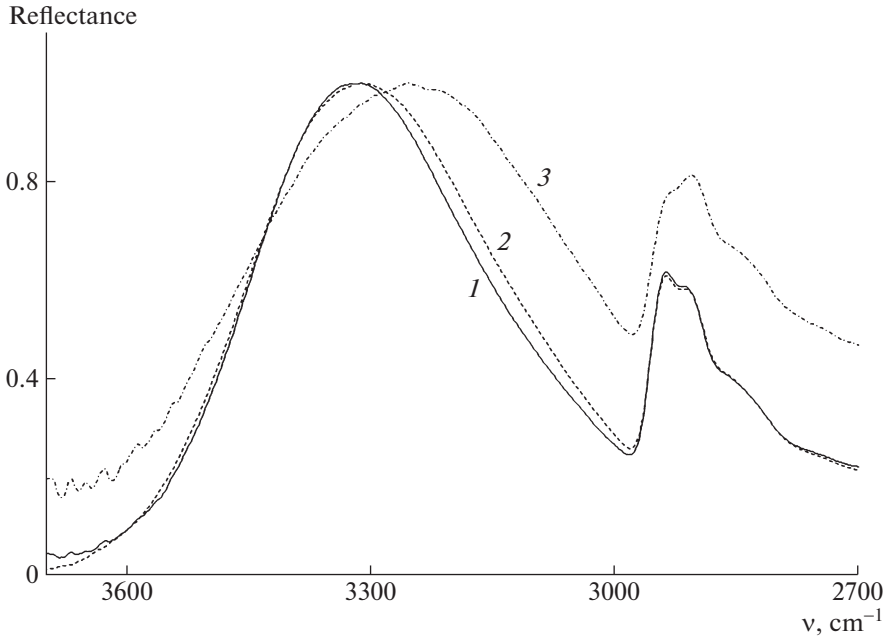

Fig. 10. The OH (3700–3000 cm^{-1}) and C–H (3000–2900 cm^{-1}) groups stretching in the ATR spectra of the CG-25 (*1*), CG-55 (*2*), and CG-85 (*3*) samples prepared with three freezing–thawing cycles ($n = 3$).

large moderately elongated pores in the gel network was ranged between 0.5 and 3.0 μm for the CG-25 sample (Fig. 11a) and between 0.5 and 4.0 μm for the CG-55 one (Fig. 11c). The network walls in the CG-55 sample were on the average thinner than those in the CG-25 sample.

The microscopy image of the CG-25 cryogel obtained at higher magnification (Fig. 11b) showed that the cryogel network consisted of spherical polydisperse nanosized formations. The spherical structures could be formed during the cooling of the 8% aqueous solution of PVA ($M \sim 10^5$) via liquid-phase separation of the system at temperature between 18 and 10°C [49]. Freezing of the heterophase system led to concentrating of the microgel particles in the space between the ice crystals, thus forming the walls of the porous system obtained upon thawing. The spherical formations were also observed in the CG-55 sample. Morphology of that sample revealed relatively uniform thickness of the network walls and more pronounced system of the interconnected pores (Fig. 11c). Besides the large pores, the network walls in the CG-25 and CG-55 samples contained numerous meso- and micropores.

Microstructure of the CG-85 sample obtained at the highest temperature of the starting PVA solution preheating (85°C) was completely different. The cellular network morphology typical of the CG-25 and CG-55 samples was not observed in the transversal fracture of the CG-85 sample at $n = 1$ (Fig. 11d). The network of the latter sample consisted of isolated fibrous formations collected in threads, with widely spaced large (up to 3–5 μm) pores between them. The cryogel network also contained the spherical elements, smaller than those in, for example, the CG-25 network. Examination of the higher-resolution microscopy image of the CG-85 sample (Fig. 11e) showed that the fibrous formations of the cryogen network also consisted of numerous touching nanosized spherical formations of different diameters.

Hence, the CG-85 network at $n = 1$ was a weakly ordered layered structure containing relatively large pores. The macropores in the CG-85 sample were formed during thawing of larger ice crystals formed at larger content (in comparison with the CG-25 and CG-55 samples) of the freely crystallized solvent in the system. Evidently, fast cooling of the PVA solution preheated at 85°C (which led to the strongest rupture of the intermolecular bonds and the thinnest hydrate shell of the macromolecules) favored the accumulation of free (freezable) water [52]. At low negative freezing temperature, that phenomenon led to the formation of larger ice crystals. Moreover, duration of the system existence in the overcooled state was shorter in the case of freezing of the hot aqueous solutions in comparison with the cold ones [53]. That fact could reduce the degree of the transition of the free water back in the bound one, crystallizing at lower temperature [54].

In the case of three freezing–thawing cycles ($n = 3$) of the hot PVA solution, the network walls became denser (Fig. 11f) and contained of densely packed (fused) spherical formations. In that case, the formed cellular structure of the CG-85 network revealed

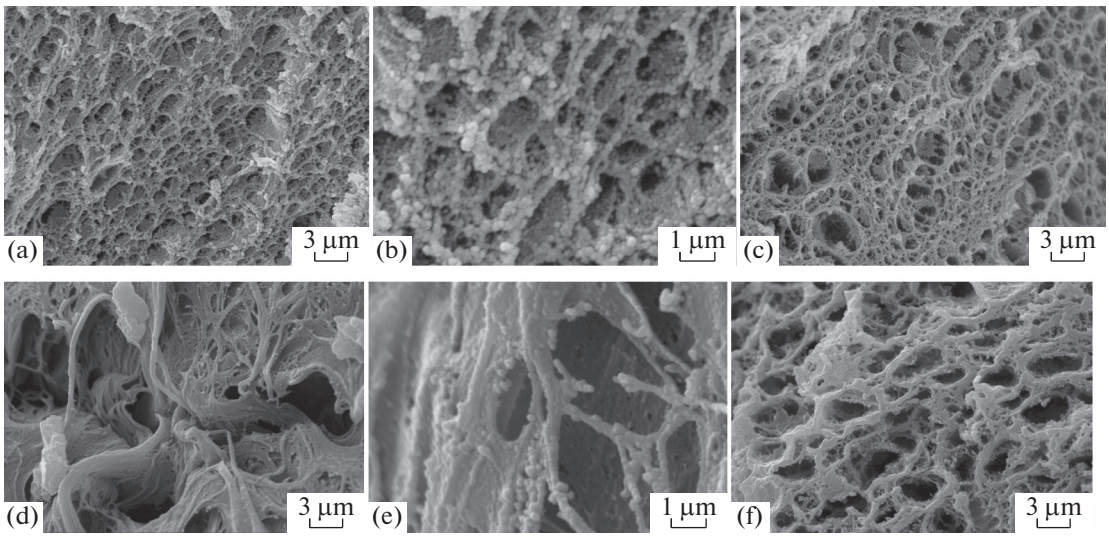

Fig. 11. Electron microscopy images of transversal fracture surface of the PVA cryogels prepared with thawing at 10°C during 24 h and preheating of the starting PVA solution at 25 (a, b), 55 (c), and 85°C (d–e). Number of the freezing–thawing cycles $n = 1$ (a–e) and 3 (f). Magnification 3500× (a, c, d, f) and 10000× (b, e).

thicker walls and higher amount of large open pores than the CG-25 and CG-55 samples. The transverse size of the pores did not exceed 3 μm, the maximum size of the pores in the cryogels formed via a single freezing–thawing.

Hence, liquid-phase separation [27] occurred during fast (~6.2 deg/min) cooling of hot (85°C) semidilute PVA solutions we well as cooling of cold (25°C) sols with rate of 4.8 deg/min, and the cryogels with the walls containing of microgel polymer particles differing in the shape, size, and degree of fusion were formed during freezing. It could be suggested that the structure of the walls of the cryogel network should be changed at higher cooling rate of the starting PVA solutions with different thermal history.

Hydrodynamic Behavior of Macroporous Cryogels Formed from the Solutions Differing in Thermal History

To assess the hydrodynamic properties of the macroporous cryogels, aqueous sol of spherical silver nanoparticles (major fraction diameter 50–60 nm [45]) was introduced in the preheated starting solutions of PVA prior to the freezing. According to the data in Fig. 12, the amount of the nanoparticles diffused from the macropores into the aqueous phase within 7 days was about 1.5 ± 0.1 times higher in the case of the CG-85 sample at $n = 1$ in comparison with the CG-55 and CG-25 samples. The highest concentration of the released nanoparticles was achieved within 3–4 days; that duration corresponded to the highest swelling of the CG-85 sample (Fig. 3a). Vigorous diffusion of the silver nanoparticles from the CG-85 sample could be due to the formation of larger macropores in that cryogel in comparison with the CG-25 and CG-55 ones. Those data coincided with the microscopy data (Fig. 11d).

In should be noted that repeated freezing–thawing treatment of the CG-85 sample filled with the stabilized silver nanoparticles led to regular decrease in the amount of the nanoparticles diffusing into the aqueous phase, down to 16–20% of the highest amount observed for $n = 1$. That effect could be due to the change in the cryogel pores size upon several freezing–thawing cycles as well as due to adsorption of the nanoparticles under conditions of increased pressure during the solvent crystallization.

Heating of semidilute aqueous PVA solutions is accompanied by several thermoreversible processes involving the hydrogen bonds: change in the thickness of the hydrate shells of the macromolecules [37, 57], their conformation state [38], character of the intermolecular interactions [58], and energy and dynamics of the water molecules not included in the hydrate shells. These processes occur simultaneously and affect each other in an aqueous solution as well as during ice crystallization [59–62] accompanied by the appearance of the intermolecular contacts which can form the crosslinks of three-dimensional network of PVA cryogels under favorable conditions.

It is generally assumed that numerous hydrogen bonds between water molecules are gradually weakened and ruptured with the increase in temperature, which leads to disordering of the water molecules location and decrease in the size of the ordered regions [40]. Dynamic properties of water molecules are changed as well. For example, the self-diffusion coefficient is increased approximately twofold with the increase in temperature from 273 to 300 K [63].

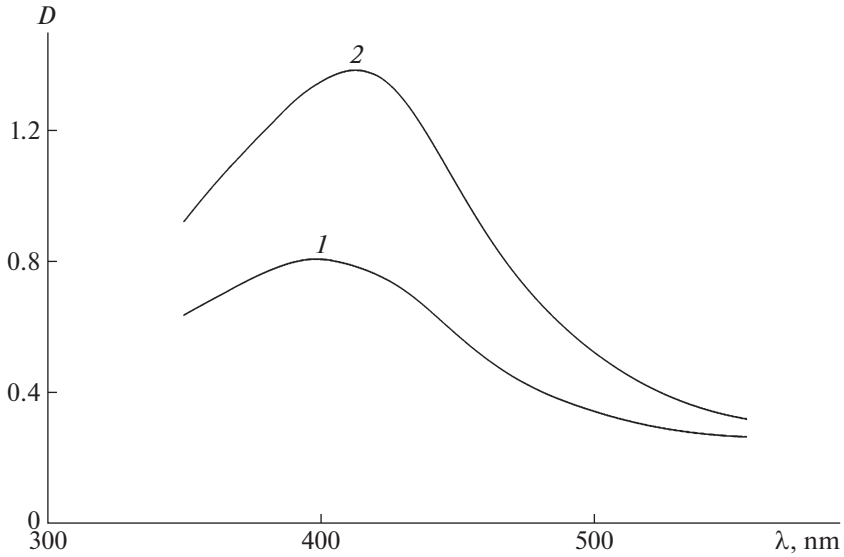

Fig. 12. Electronic absorption spectra of stabilized silver nanoparticles released into water via diffusion from the CG-55 (*1*) and CG-85 (*2*) ($n = 1$) gel macropores at room temperature during 7 days.

Cooling below 4°C leads to the decrease in density and increase in molar volume of water, accompanied by the ordering of the hydrogen bonds in the tetragonal structure [40]. However, the change in thermodynamic parameters of water molecules and transformation of tetrahedral hydrogen bonds into their more stable form—hexagonal ice structure Ih—are observed at the temperature range preceding the phase transition into ice, in overcooled water. Heating of the crystallized system to the melting point of the Ih ice crystals (273 K) leads to the appearance of liquid fraction of the ice-like hexamer clusters in water [64, 65]. The experiments have revealed that the "thawed water" at 25°C [66] can exist in the metastable state during up to 1 day.

Temperature of ice crystallization and dynamic properties of water molecules depend on the character of their hydrogen bonding with macromolecules (Fig. 13) [52] as well as between each other and are determined (among other factors) by the distance to the macromolecules surface [62]. The amount of water non-freezable during cooling of a PVA solution is independent of the thermal history preceding the freezing, in contrast to the fractions of bound and free water [57]. Water properties in the hydrate shell are strongly different from these of free water, for example, in lower molecules mobility and crystallization temperature.

The presence of hydrophilic PVA macromolecules in a solution decelerates the motion of weakly bound water molecules to the centers of ice crystallization [67]. Moreover, structural features of PVA determine their antifreezing action consisting in adsorption of isolated macromolecules on the ice crystallization centers [68]. Such action is enhanced by adsorption of large aggregates of PVA macromolecules [69] blocking many growing crystallization sites. Preheating of a PVA solution prior to the freezing affects the amount of water molecules bound to the macromolecules as well as their conformation and association. Hence, isolated macromolecules with lower amount of weakly bound water (as in the case of hot PVA solutions) apparently exhibit less prominent antifreezing properties.

The formation of larger ice crystals during fast cooling of the hot PVA solution was indirectly evidenced by faster diffusion of the silver nanoparticles from the macropores of the CG-85 sample ($n = 1$) in comparison with the CG-25 and CG-55 ones. It could be suggested that deterioration of the antifreezing properties of smaller and less hydrated individual PVA macromolecules at 85°C in comparison with those of bulky associates of macromolecules at 55 and 25°C was among the factors of the formation of larger ice crystals upon freezing of the hot PVA solution (Fig. 11d).

The conditions of prolonged keeping of the thawed samples at low positive temperature affected the properties of the formed cryogels as well. However, even favorable conditions of thawing could not promote the growth of the microcrystallites in the absence of nuclei in the starting systems. It has been found that the number of hydrogen bonds between PVA macromolecules and water molecules at 300 K is 13–14 times higher than that of the intermolecular hydrogen bonds [74]. The mobility of functional groups of the macromolecules observed at subzero temperature is enough for the formation of amorphous intermolecular contacts through the water molecules layer [70]. The formation of microcrystallites requires the mobility of the macromolecular segments arranged in parallel [24]

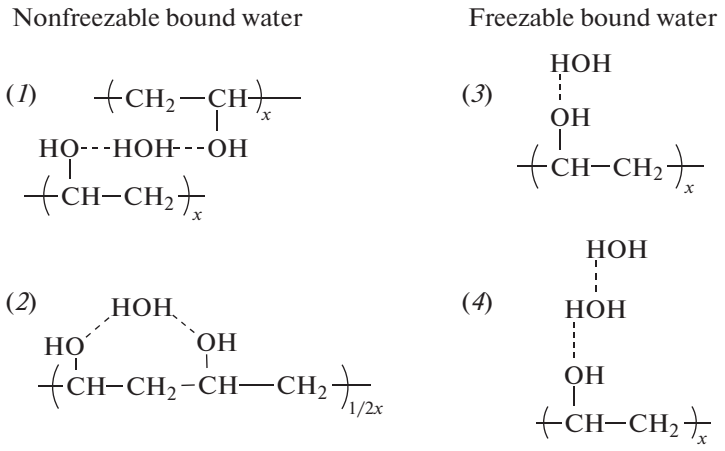

Fig. 13. Possibilities of the formation of hydrogen bonds in the PVA–water system: *1*—intermolecular hydrogen bonds involving water molecules, *2*—intramolecular hydrogen bonds involving water molecules, *3*—the bonds between the OH group of PVA and a water molecule, *4*—the bonds between the OH group of PVA and two water molecules.

and linked via the hydrogen bonds not involving hydrating water [25], under conditions of minimal hydration of the macromolecules. If the dehydration is not sufficiently pronounced, the formation of intermolecular hydrogen bonds not involving water molecules is restricted.

The conditions favoring the formation and growth of the microcrystallites are created at temperature close to the devitrification of the frozen polymer system (about 10°C as per the TMA data). At the same time, the hydrogen bonds are still partially preserved in the structure of the hexagonal ice-like clusters upon thawing of the Ih ice crystals [65]. Hence, certain amount of liquid hexagonal water clusters in the gel do not exhibit tetrahedral coordination typical of liquid water in the gel during the thawing at low positive temperature. This feature of water structure is also affected by the steric hindrance imparted by the polymer chains [71]. Rearrangement of the hexagonal ice-like clusters into the tetrahedral ones, typical of liquid water, at 0–25°C can to certain extent be regarded as the continued melting of the Ih ice crystals. The existence of part of free water molecules in the form of low-mobile hexagonal clusters at low positive temperature restricts their ability to form hydrogen bonds with the macromolecules (hydration) [57]. For example, only half of 12 hydrogen atoms of the hexagonal $(H_2O)_6$ cluster are in the free state, capable of the hydrogen bonding with the macromolecules. This fact favor the formation of microcrystalline crosslinks in the gel network, since it is known that the interaction of water molecules with the hydroxyl groups of PVA macromolecules can even reduce the degree of microcrystallinity [72]. It is accompanied by the rupture of the hydrogen bonds between the hydroxyl groups of the macromolecules, and the configuration of crystalline planar zigzag is transformed into the amorphous configuration. As a result, prolonged keeping of the thawed samples at the devitrification temperature under conditions of minimal hydration of the macromolecules promotes the formation and growth of the microcrystallite nuclei.

In summary, preheating of the starting 8% aqueous solution of PVA at 25, 55, and 85°C followed by immediate cooling to temperature below the glass transition and freezing points, keeping in the frozen state, and slow thawing at temperature about 10°C corresponding to devitrification of the frozen system affected the morphology, physico-chemical properties, and the balance of amorphous and crystalline features of the PVA cryogels.

CONCLUSION

Preheating of 8% aqueous sol of PVA at 20–90°C led to stepwise decrease in the system turbidity related to the change in the aggregate state of the macromolecules due to the decrease in the amount of intermolecular hydrogen bonds and the microcrystallinity regions as well as weakening of the hydrophobic interactions.

The cryogels with elastoplastic properties nonuniform over the specimen volume were formed during fast and predominantly unidimensional cooling and freezing of the preheated PVA solutions and subsequent thawing at low positive temperature; the mechanical properties turned uniform during the ageing at room temperature.

Degree of the PVA cryogels swelling in water was directly related with temperature of preheating of the starting solution prior to freezing as well as duration of the thawed keeping at the devitrification temperature (about 10°C) and inversely related to the number of the freezing–thawing cycles.

Higher amount of stabilized silver nanoparticles (d = 50–60 nm) released in water via diffusion from the filled CG-85 sample (n = 1) evidenced larger size of the pores in that gel in comparison with the CG-25 and CG-55 ones.

The ATR IR spectroscopy investigation revealed that PVA macromolecules existing in the dissociated state during heating of the solution at 85°C formed the strongest network of the hydrogen bonds upon subsequent cryotropic impact (n = 3).

Electron microscopy data on the morphology of the CG-25 and CG-55 samples obtained at n = 1 revealed fine cellular structure formed of the microgel spherical particles, and the morphology of the CG-85 sample at n = 1 showed more widely spaced large (up to 3–5 μm) pores and thick walls in the form of multiple polymer fibers consisting of the spherical microgel particles. At n = 3, the CG-85 sample revealed the cellular structure as well, with the denser walls consisting of "fused" microgel spherical particles.

It was shown that morphology, physico-chemical properties, and the presence of microcrystalline crosslinks in the network of PVA cryogels were affected on the thermal impact on PVA macromolecules in the starting aqueous solutions, besides the temperature-duration conditions of the cryogenic structuring.

ACKNOWLEDGMENTS

The experiments on the formation of poly(vinyl alcohol) hydrogels, investigation of their structure and the effect of thermal treatment on the properties were performed at the Institute of Organoelement Compounds, Russian Academy of Sciences. Calculations and interpretation of the transitions in the thermomechanical curves were performed at Moscow State University of Civil Engineering.

Authors are grateful to A.G. Bogdanov (MSU) for the assistance in the scanning electron microscopy imaging of the objects.

FUNDING

This study was financially supported by the Ministry of Science and Higher Education of Russian Federation (project "Theoretical-Experimental Engineering of Novel Composite Materials for Safe Maintenance of Buildings and Constructions Under Conditions of Technogenic and Biogenic Hazards," no. FSWG-2020-0007) (MSUCE) and the State Contact (no. 0085-2019-0004, IOC RAS).

CONFLICT OF INTEREST

The authors declare that they have no conflicts of interest.

REFERENCES

1. *Hydrogels in Medicine and Pharmacy*, Vol. 1, Ed. by N. A. Peppas (CRC Press, New York, 2019).
2. Ch. M. Hassan and N. A. Peppas, Macromolecules **33**, 2472 (2000).
3. *Polymeric Cryogels Macroporous Gels with Remarkable Properties*, Ed. by O. Okay (Springer, New York, 2014).
4. *Polymeric Gels. Characterization, Properties and Biomedical Applications*, Ed. by K. Pal and I. Banerjee (Elsevier, Cambridge, 2018).
5. *Biomedical Hydrogels Biochemistry, Manufacture and Medical Applications*, Ed. by S. Rimmer (Woodhead Publ. Ltd., Oxford, Cambridge, 2011).
6. N. A. Peppas, J. Z. Hilt, A. Khademhosseini, and R. Langer, Adv. Mater. **18**, 1345 (2006).
7. H. Levine, and L. Slade, *Water Relationships in Food* (Springer, New York 1991).
8. Ch. M. Hassan and N. A. Peppas, Adv. Polym. Sci. **153**, 65 (2000).
9. R. S. Harland and N. A. Peppas, J. Pharm. Sci. **78** (2), 146 (1989).
10. B. V. Slaughter, Sh. S. Khurshid, O. Z. Fisher, A. Khademhosseini, and N. A. Peppas, Adv. Mater. **21**, 3307 (2009).
11. M. Kobayashi, J. Toguchida, and M. Oka, Biomaterials **24** (4), 639 (2003).
12. M. I. Baker, S. P. Walsh, Z. Schwartz, and B. D. Boyan, J. Biomed. Mater. Res. **100B**, 1451 (2012).
13. *Biomaterials for Treating Skin Loss*, Ed. by D. Orgill and C. Blanco (CRC Press Woodhead Publ. Ltd., Cambridge, 2009).
14. S.-H. Hyon, W.-I. Cha, Y. Ikada, M. Kita, Y. Ogura, and Y. Honda, J. Biomater. Sci., Polym. Ed. **5** (5), 397 (1994).
15. A. Kumar and S. S. Han, Int. J. Polym. Mater. Polym. Biomater. **66** (4), 159 (2017).
16. M. Teodorescu, M. Bercea, and S. Morariu, Polym. Rev. **58** (2), 247 (2018).
17. L. Dai and Sh. Yu, Polym. Adv. Technol. **14**, 449 (2003).
18. V. I. Lozinsky, Russ. Chem. Rev. **67**, 573 (1998).
19. W. Wan, A. D. Bannerman, L. Yang, and H. Mak, Adv. Polym. Sci. **263**, 283 (2014).
20. Ph. Molyneux, *Water-Soluble Synthetic Polymers: Properties and Behavior* (CRC Press, Boca Raton London, New York, 1984).
21. J. L. Valentin, D. Lopez, R. Hernandez, C. Mijangos, and K. Saalwachter, Macromolecules **42**, 263 (2009).
22. V. I. Klenin, O. V. Klenina, V. A. Kolchanov, B. I. Shvartsburd, S. Ya. Frenkel', Vysokomol. Soedin., Ser. A **16** (10), 2351 (1974).
23. T. Nakaoki and H. Yamashita, J. Mol. Struct. **875**, 282 (2008).
24. Bartenev, G.M. and Frenkel', S.Ya., *Fizika Polimerov* (Physics of Polymers) (Khimiya, Leningrad, 1990) [in Russian].
25. R. Hodge, G. Edward, and G. Simon, Polymer **37** (8), 1371 (1996).
26. H. Hatakeyama and T. Hatakeyama, Thermochim. Acta **308**, 3 (1998).
27. K. Kawanishi, M. Komatsu, and T. Inoue, Polymer **28**, 980 (1987).

28. E. Otsuka, M. Sugiyama, and A. Suzuki, J. Phys.: Conf. Ser. **247**, 1 (2010).

29. T. Kanaya, N. Takahashi, H. Takeshita, M. Ohkura, K. Nishida, and K. Kaji, Polym. J. **44**, 83 (2012).

30. O. N. Tretinnikov and S. A. Zagorskaya, J. Appl. Spectroscopy **78** (6), 904 (2012).

31. A. Bhattacharya and P. Ray, J. Appl. Polym. Sci. **93**, 122 (2004).

32. *Water Soluble Polymers*, Ed. by Z. Amjad (Plenum Press, New York, 1998).

33. *Polymeric Cryogels. Macroporous Gels with Remarkable Properties. Advances in Polymer Science, 263,* Ed. by O. Okay (Springer Int. Publ., Switzerland, 2014).

34. N. A. Peppas and E. W. Merrill, J. Appl. Polym. Sci. **21**, 1763 (1977).

35. K. Arai, M. Okuzono, and T. Shikata, Macromolecules **48** (5), 1573 (2015).

36. G. Paradossi, I. Finelli, F. Natali, M. T. F. Telling, and E. Chiessi, Polymers **3**, 1805 (2011).

37. Ch. Wu, Polymer **51**, 4452 (2010).

38. V. J. Klenin and I. V. Fedusenko, Polym. Sci., Ser. A **45** (12), 1231 (2003).

39. O. V. Khorolskyi, Ukr. J. Phys **63** (2), 144 (2018).

40. *Water: Structure, State, Solvation*, Ed. by A. M. Kutepova (Nauka, Moscow, 2003) [in Russian].

41. L. Zhao, K. Ma, and Z. Yang, Int. J. Mol. Sci. **16**, 8454 (2015).

42. T. Hatakeyama, F. X. Quinn, and H. Hatakeyama, Carbohydr. Polym. **30**, 155 (1996).

43. D. R. Moberg, D. Becker, Ch. W. Dierking, F. Zurheide, B. Bandow, U. Buck, A. Hudait, V. Molinero, F. Paesani, and T. Zeuch, Proc. Natl. Acad. Sci. USA (PNAS) **116**, 24413 (2019).

44. V. I. Lozinsky, E. S. Vainerman, L. V. Domotenko, A. M. Mamtsis, E. F. Titova, E. M. Belavtseva, and S. V. Rogozhin, Colloid Polym. Sci. **264**, 19 (1986).

45. N. Samoilova, E. Kurskaya, M. Krayukhina, A. Askadsky, and I. Yamskov, J. Phys. Chem. B **113**, 3395.

46. V. A. Kargin and T. I. Sogolova, Zh. Fiz. Khim. **23**, 540 (1949).

47. E. H. Lee and J. R. Radok, J. Appl. Mech. E **27**, 438 (1960).

48. Sh. Agnihotri, S. Mukherji, and S. Mukherji, RSC Adv. **4**, 3974 (2014).

49. C. Hara and M. Matsuo, Polymer **36** (3), 603 (1995).

50. P. J. Willcox, D. W. Howie, K. Schmidt-Rohr, D. A. Hoagland, S. P. Gido, S. Pudjijanto, L. W. Kleiner, and S. Venkatraman, J. Polym. Sci., Polym. Phys. Ed. **37**, 3438 (1999).

51. T. Hatakeyema, J. Uno, Ch. Yamada, A. Kishi, and H. Hatakeyama, Thermochim. Acta **431**, 144 (2005).

52. W. Li, F. Xue, and R. Cheng, Polymer **46**, 12026 (2005).

53. J. D. Brownridge, Am. J. Phys. **79** (1), 78 (2011).

54. T. Hatakeyama, M. Tanaka, and H. Hatakeyama, J. Biomater. Sci., Polym. Ed. **21**, 1865 (2010).

55. T. Hatakeyama, A. Yamauchi, and H. Hatakeyama, Eur. Polym. J. **23**, 361 (1987).

56. N. A. Peppas and E. W. Merrill, J. Polym. Sci. **14**, 441 (1976).

57. E. Chiessi, F. Cavalieri, and G. Paradossi, J. Phys. Chem. B **109** (16), 8091 (2005).

58. V. J. Klenin, *Thermodynamics of Systems Containing Flexible-Chain Polymers* (Elsevier, Amsterdam, 1999).

59. S. Ogawa, M. Koga, and S. Osanai, Chem. Phys. Lett. **480**, 86 (2009).

60. T. Inada and S.-S. Lu, Chem. Phys. Lett. **394**, 361 (2004).

61. P. M. Naullage and V. Molinero, J. Am. Chem. Soc. **142**, 4356 (2020).

62. S. Wu, Z. He, J. Zang, Sh. Jin, Z. Wang, J. Wang, Y. Yao, and J. Wang, Sci. Adv. **5**, 1 (2019).

63. S. K. Reddy, S. C. Straight, P. Bajaj, C. H. Pham, M. Riera, D. R. Moberg, M. A. Morales, C. Knight, A. W. Gotz, and F. Paesani, J. Chem. Phys. **145**, 194504-1 (2016).

64. A. V. Khakhalin, O. N. Gradoboeva, and Ya. N. Shirshov, Moscow Univ. Phys. Bull. **67** (6), 537 (2012).

65. J. Liu, X. He, and J. Z. H. Zhang, Phys. Chem. Chem. Phys. **19**, 11931 (2017).

66. A. Kholmanskiy, J. Mol. Struct. **1989**, 124 (2015).

67. D. Laage, G. Strinemann, and J. T. Hynes, Sci. China: Phys., Mech. Astron. **53** (6), 1068 (2010).

68. P. M. Naullage and V. Molinero, J. Am. Chem. Soc. **142**, 4356 (2020).

69. L. Weng, S. L. Stott, and M. Toner, Langmuir **34** (17), 5116 (2017).

70. V. I. Lozinsky and L. G. Damshkaln, J. Appl. Polym. Sci. **77**, 2017 (2000).

71. Y. Tamai and H. Tanaka, Phys. Rev. E: **59** (5), 5647 (1999).

72. S. K. Mallapragada and N. A. Peppas, J. Polym. Sci., Polym. Phys. Ed. **34**, 1339 (1996).

73. W. Li, F. Xue, and R. Cheng, Polymer **46**, 12026 (2005).

74. L. Shi and Q. Han, Mol. Simul. **44** (17), 1363 (2018).

75. F. Auriemma, C. De Rosa, and R. Triolo, Macromolecules **39**, 9429 (2006).

Translated by E. Karpushkin